Journal of Math-for-industry, Vol.2(2010B-7), pp.171–181

Math-for-industry
Education & Research Hub

Multiscale sulfate attack on sewer pipes: Numerical study of a fast micro-macro mass transfer limit

Vladimír Chalupecký, Tasnim Fatima, and Adrian Muntean

Received on July 15, 2010 / Revised on September 29, 2010

Abstract. We present two multiscale reaction-diffusion (RD) systems modeling sulfate attack in concrete structures (here: sewer pipes). The systems are posed on two different spatially separated scales. The only difference between them is the choice of the *micro-macro transmission condition*. We explore numerically the way in which the macroscopic Biot number Bi^M connects the two reaction-diffusion scenarios. We indicate connections between the solution of the "regularized" system (with moderate size of Bi^M) and the solution to the "matched" system (with blowing up size of Bi^M), where Henry's law plays the role of the micro-macro transmission condition.

Keywords. Multiscale RD system, micro-macro transmission conditions, sulfate corrosion, acid attack, modeling of concrete, finite difference scheme, convergence rates

Abbreviations. RD – reaction-diffusion; PDEs – partial differential equation(s); ODEs – ordinary differential equation(s); EOC – experimental order of convergence

1. Introduction

In this paper, we deal with the problem of corrosion of concrete sewer pipes (and other structures made of concrete) that sustain the attack of aggressive compounds like sulfuric acid. In the context of mathematical modeling of concrete corrosion, the general objective is to develop models that can give reliable predictions on the rate of corrosion and on the speed of an advancing corrosion front separating corroded and undamaged concrete.

Concrete is a material with porous structure – it can be viewed as consisting of a solid matrix and a system of interconnected pores and fissures, which are partly filled with water. Böhm et al. [4] describe this structure for the gypsum layer formed as a product of sulfatation reactions. There are two scales related inherently to the size of the air and water phase and to the chemical reactions taking place there. The network of pores allows for a fast diffusion of gaseous compounds (like H_2S in the case of sewer pipes) throughout the air phase on the macroscopic scale. On the other hand, diffusion (and chemical reactions) in the water phase are limited by the size of pores and thus take place at a much smaller, microscopic scale. This scenario indicates that one really needs to get a sound understanding of *structured transport* – since this is the main mechanism responsible for a significant interplay between micro (pore level) and macro (pipe level) scales. These considerations[1] motivate our multiscale approach to this corrosion process.

[1]Additionally, such a two-scale (micro-macro) approach can be motivated and mathematically justified for a special scaling via periodic homogenization, for instance, cf. [11] but also [8, 15, 16] and references cited therein.

The main focus of this paper is to study the role of two *micro-macro transmission conditions*. In order to do this we look for the numerical solution of two multiscale partly dissipative reaction-diffusion systems modeling sulfate attack that are derived via homogenization in [9]. These systems are posed on two different spatially separated scales, the only difference between them being the choice of the micro-macro transmission condition imposed at the air-water interface. The multiscale nature of the model allows us to perform computations at macroscopic length scales that are relevant to practical applications while taking into account transport and reactions occurring at very small scales. At this point, the relevant scientific questions are: (i) How can one bridge the micro information to the macro one? (ii) Are there other alternatives? (iii) Which is the right one?

Here we choose to deal with question (i). Namely, we explore numerically the way in which the macroscopic Biot number Bi^M connects the two reaction-diffusion scenarios mentioned before. Furthermore, we hope to be able to find relations between the solution of the "regularized" system (with moderate size of Bi^M) and the solution to the "matched" system (with blowing up size of Bi^M), where Henry's law plays the role of the micro-macro transmission condition.

The paper is organized as follows: Descriptions of the involved chemistry and basic geometry are given in sections 1.1 and 2.1, respectively. The two-scale model equations are outlined in 2.2 and their well-posedness is addressed in section 2.3. The bulk of the paper is contained in section 3 and section 4. We close the paper with section 5 that

includes a brief discussion of a couple of open multiscale questions that we wish to address as next step.

1.1. Basic description of the chemistry

Sulfuric acid (H_2SO_4) is one of the most aggressive acids that can come in contact with concrete structures. It destroys the strength of the concrete completely and causes spalling and material corrosion. The chemical picture is rather simple: Active anaerobic bacteria existing in the waste water produce gaseous H_2S which moves in the air space of the pipe and goes up towards the pipe wall. Then gaseous H_2S enters into the concrete pores (microstructures) via both air and water parts.

Once arrived inside the microstructure, H_2S diffuses within the available air space and dissolves in the thin (stationary) water film clinging on the wall of the fabric. In sewer pipes with increased temperature (e.g., in a hot climate), sulfate-rich environments rapidly lead to the formation of sulfuric acid by the action of aerobic bacteria living in the water film. This aggressive acid reacts with calcium carbonate (i.e., with our concrete sample) and produces gypsum.

We pay special attention to the following aspects:

- exchange of H_2S from water to the air phase and vice versa (see [2] for more comments on mass transfer across air-liquid interfaces);
- production of gypsum at micro solid-water interfaces.

The transfer of H_2S is modeled here by means of the Henry's law, while the production of gypsum ($CaSO_4 \cdot 2H_2O$) is incorporated in a non-standard non-linear reaction rate, here denoted as η; see (3) for a precise choice. Equation (4) indicates the linearity of the Henry's law structure we have in mind. The standard reference for modeling gas-liquid reactions at stationary interfaces (including a derivation of the Henry's law) is [7].

There are many chemical reactions taking place in the pores of sewer pipes which degrade the performance of the pipe structure depending on the intensity of the interaction between the chemical reactions and the local environment. Here we focus our attention on the following few relevant chemical reactions:

$$\text{(1a)}\quad 10H^+ + SO_4^{-2} + \text{organic matter} \to H_2S(\text{aq}) + 4H_2O + \text{oxidized matter}$$

$$\text{(1b)}\quad H_2S(\text{aq}) + 2O_2 \to 2H^+ + SO_4^{2-}$$

$$\text{(1c)}\quad H_2S(\text{aq}) \rightleftharpoons H_2S(\text{g})$$

$$\text{(1d)}\quad 2H_2O + H^+ + SO_4^{2-} + CaCO_3 \to HCO_3^- + CaSO_4 \cdot 2H_2O.$$

It is worth mentioning, at this point, that if this is needed we can extend our multiscale models with minimal effort to more complex chemical reactions.

1.2. Related literature

From the modeling viewpoint, we are very much inspired by the comprehensive description of the sulfate corrosion mechanisms relevant for sewage systems as presented in [4, 12, 13]. Note that in the *loc. cit.* papers, the authors proposed macroscopic PDE models to capture the motion of a macroscopic corrosion front penetrating sewer pipes – the modeling tool is a moving-boundary strategy. From a different perspective[2], mathematically sound macroscopic approaches of sulfatation of carbonated stones (especially connected with conservation of historical heritage) are reported by Aregba-Driollet et al. in [1] and references therein.

Standard reference works regarding cement chemistry are refs. [10, 26]. For a detailed description of the mechanisms leading to sulfate corrosion in concrete, we refer the readers to standard civil engineering literature like [3, 14, 21, 25, 27], or [22]. It is worth noting that there is a lot of literature on sulphate attack. For instance, a lot of modeling work has been done by K. Scrivener and coworkers at the EPFL in Lausanne, F. Glasser in Aberdeen, F. Schmid-Döhl, E. Rigo (the software Transreac) in Hamburg. They all use a Gibbs energy minimization approach. The major issue when choosing this modeling alternative is that one cannot investigate anymore transport effects. To fill this gap, E. Beddoe, W. Dörner and collaborators from TU München use the code PHREEQC not only because it has a huge data base and is easy to use, but also because it seems that it can take diffusion of the various species into account.

None of these approaches is able to cope with the *inherent multiscale geometry* of the pore matrix. This is the place where we wish to contribute with our mathematical understanding of two-spatial-scale systems; compare [16, 18, 20] and also [8, 15].

2. Two-scale model for sulfate attack

2.1. Basic two-scale geometry

We consider a sewer pipe made of partially wet concrete. Focusing on the already damaged part of the concrete, we consider a single critical macroscopic region $\Omega := (0, L)$ (with $L > 0$) representing a concrete sample along a line perpendicular to the pipe surface, where corrosion initiates, and aim to follow the space-time evolution of the damage. The boundary of Ω, say Γ, is composed of two disjoint parts $\Gamma^D := \{0\}$ (the inner surface of the pipe) and $\Gamma^N := \{L\}$, the Dirichlet and the Neumann boundaries. As typical microstructure (or standard cell [11]) we take $Y := (0, \ell)$ (with $\ell > 0$).

Usually cells in concrete contain a stationary water film, and air and solid fractions in different ratios depending on the local porosity. Generally, we expect that the choice of the microstructure depends on the macroscopic position

[2]The approach taken in [1] is line with fast-reaction limits and related regularizations of Stefan-like free boundary problems.

$x \in \Omega$, i.e., we would then have Y_x; see [9] for more comments in this direction directly related to this sulfatation problem and [15] for a rather general RD setting posed in heterogeneous (x-dependent) domains. Here we assume that the medium Ω is made by periodically repeating the *same* microstructure Y (Ω is a perfectly periodically paved region). Furthermore, since at the microscopic level the involved reaction and diffusion processes take place in pore water, we choose to denote by Y only the wet part of the pore.

Finally, let S be the time interval $(0,T)$ (with $T > 0$) during which we consider the process. As a rule Δ_y denotes the Laplacian incorporating partial derivatives only w.r.t. the variable $y \in Y$, while Δ will be the Laplacian referring only to the partial derivatives w.r.t. the variable $x \in \Omega$. A similar rule defines ∂_x and ∂_y.

2.2. Outline of two-scale model equations

We consider the following two-scale system of PDEs and one ODE for unknown functions

$$
\begin{aligned}
&w_1 : \Omega \times Y \times S \to \mathbb{R} && \text{– concentration of } H_2SO_4,\\
&w_2 : \Omega \times Y \times S \to \mathbb{R} && \text{– concentration of } H_2S(aq),\\
&w_3 : \Omega \times S \to \mathbb{R} && \text{– concentration of } H_2S(g),\\
&w_4 : \Omega \times Y \times S \to \mathbb{R} && \text{– concentration of moisture,}\\
&w_5 : \Omega \times \{y=\ell\} \times S \to \mathbb{R} && \text{– concentration of gypsum,}
\end{aligned}
$$

such that

$$
\begin{aligned}
&\text{(2a)} && \beta_1\partial_t w_1 - \beta_1 d_1 \Delta_y w_1 = -\Phi_1^2 k_1 w_1 + \Phi_2^2 k_2 w_2, && \text{in } \Omega\times Y\times S,\\
&\text{(2b)} && \beta_2\partial_t w_2 - \beta_2 d_2 \Delta_y w_2 = \Phi_1^2 k_1 w_1 - \Phi_2^2 k_2 w_2, && \text{in } \Omega\times Y\times S,\\
&\text{(2c)} && \partial_t w_3 - d_3\Delta w_3 = -Bi^M\left(Hw_3 - w_2|_{y=0}\right), && \text{in } \Omega\times S,\\
&\text{(2d)} && \beta_4\partial_t w_4 - \beta_4 d_4 \Delta_y w_4 = k_1 w_1, \text{ in } \Omega\times Y\times S,\\
&\text{(2e)} && \beta_5\partial_t w_5 = +\Phi_3^2\eta(w_1,w_5), && \text{in } \Omega\times\{y=\ell\}\times S,
\end{aligned}
$$

where $\beta_k > 0$, $k \in \{1,2,4,5\}$, are parameters, $d_k > 0$, $k \in \{1,2,3,4\}$, are the diffusion coefficients, Bi^M is a dimensionless Biot number [28], and $k_k : Y \to \mathbb{R}$, $k \in \{1,2,3\}$, are functions modeling the rate "constants". We assume the reaction rate η takes the form

$$
\text{(3)} \qquad \eta(\alpha,\beta) = \begin{cases} k_3\alpha^p(\bar{c}-\beta)^q, & \text{if } \alpha \geq 0,\ \beta \geq 0,\\ 0, & \text{otherwise,}\end{cases}
$$

where $\bar{c}$ is a known equilibrium constant concentration and $p \geq 1, q \geq 1$ are the partial orders of reaction. The Φ_k^2, $k \in \{1,2,3\}$, are Damköhler numbers [28] corresponding to three distinct chemical mechanisms (reactions). They are dimensionless numbers that compare the characteristic time of the fastest transport mechanism (here: the diffusion of H_2S in the gas phase) to the characteristic timescale of the k-th chemical reaction. It is worth noting that terms like

$$
\text{(4)} \qquad Bi^M\left(Hw_3(t,x) - w_2(t,x,y=0)\right)
$$

are usually referred to in the literature as production terms by Henry's or Raoult's law; see [7]. $H > 0$ is the Henry's constant. The special feature of our scenario is that now the term (4) *bridges* two distinct spatial scales: one macro with $x \in \Omega$ and one micro with $y \in Y$.

The system (2) is supplemented with initial and boundary conditions, which read as

$$
\begin{aligned}
&\text{(5a)} && -d_1\partial_y w_1 = 0, && \text{on } \Omega\times\{y=0\}\times S,\\
&\text{(5b)} && -d_1\partial_y w_1 = +\Phi_3^2\eta(w_1,w_5), && \text{on } \Omega\times\{y=\ell\}\times S,\\
&\text{(5c)} && -d_2\partial_y w_2 = -Bi^M(Hw_3 - w_2), && \text{on } \Omega\times\{y=0\}\times S,\\
&\text{(5d)} && -d_2\partial_y w_2 = 0, && \text{on } \Omega\times\{y=\ell\}\times S,\\
&\text{(5e)} && w_3 = w_3^D, && \text{on } \Gamma^D\times S,\\
&\text{(5f)} && -d_3\partial_x w_3 = 0, && \text{on } \Omega\setminus\Gamma^D\times S,\\
&\text{(5g)} && -d_4\partial_y w_4 = 0, && \text{on } \Omega\times\{y=0\}\times S,\\
&\text{(5h)} && -d_4\partial_y w_4 = 0, && \text{on } \Omega\times\{y=\ell\}\times S.
\end{aligned}
$$

Note that the "information" at the microscale is connected to the macroscale situation via the right-hand side of (2c) and via the micro-macro transmission condition (5c). Remark that all involved parameters (except for H, d_3 and Bi^M) contain microscopic information. The coefficients d_3 and Bi^M are effective ones (see [9] for a way of calculating them), while H can be read off from existing macroscopic experimental data. For more modeling details, we refer the reader to [4, 9] and references cited therein.

We refer to (2a)–(5h) as problem (P).

2.3. Well-posedness of problem (P)

Let us assume the following restrictions on data and parameters:

(A1) $d_i > 0$ ($i \in \{1,\dots,4\}$), $\beta_j > 0$ (for $j \in \{1,2,4,5\}$), $\Phi_l^2 > 0$ (for $l \in \{1,2,3\}$);

(A2) The reaction term $\eta : \mathbb{R}\times\mathbb{R} \to \mathbb{R}_+$ is globally Lipschitz with respect to both variables;

(A3) $w_3^D \in H^1(S,H^2(\Omega)) \cap H^2(S,L^2(\Omega)) \cap L^\infty_+(S\times\Omega)$, $w_{30} \in H^2(\Omega)\cap L_+(\Omega)$, $w_{30} - w_3^D \in H_0^1(\Omega)$, $w_{p0} \in L^2(\Omega;H^2(Y)) \cap L^\infty_+(\Omega\times Y)$ (for $p \in \{1,2,4\}$), and $w_{50} \in L^2(\Omega\times\{y=\ell\}) \cap L^\infty_+(\Omega\times\{y=\ell\})$.

Let us introduce the set of indices $\mathcal{I} := \{1,2,4\}$ as well as the functions $F_i : \mathbb{R}^3 \to \mathbb{R}$ defined by

$$
\begin{aligned}
&\text{(6)} && F_1(r) := -\Phi_1^2 k_1 r_1 + \Phi_2^2 k_2 r_2,\\
&\text{(7)} && F_2(r) := \Phi_1^2 k_1 r_1 - \Phi_2^2 k_2 r_2,\\
&\text{(8)} && F_3(r) := k_1 r_1,
\end{aligned}
$$

for all $r := (r_1,r_2,r_3) \in \mathbb{R}^3$.

Our concept of weak solution is as follows:

Definition 1. The vector of functions

$$(w_1, w_2, w_3, w_4, w_5)$$

with $w_3 - w_3^D \in L^2(S, H_0^1(\Omega))$, $\partial_t w_3 \in L^2(S \times \Omega)$, $w_i \in L^2(S, L^2(\Omega, H^1(Y)))$, $\partial_t w_i \in L^2(S \times \Omega \times Y)$ for all $i \in \mathcal{I}$, and $w_5(\cdot, x, y) \in H^1(S)$ for a.e. $(x, y) \in \Omega \times Y$, is called *weak solution* to problem (P) if for a.e. $t \in S$ the following identities hold:

$$\int_\Omega \partial_t w_3 \varphi_3 + d_3 \int_\Omega \nabla w_3 \nabla \varphi_3 = -\int_\Omega \nabla_y w_2|_{y=0} \varphi_3,$$

$$\sum_{i\in\mathcal{I}} \beta_i \int_\Omega \int_Y \partial_t w_i \varphi_i + \sum_{i\in\mathcal{I}} \beta_i d_i \int_\Omega \int_Y \nabla_y w_i \nabla_y \varphi_i = \sum_{i\in\mathcal{I}} \int_\Omega \int_Y F_i(w)\varphi_i,$$

and

$$\beta_5 \partial_t w_5 = +\Phi_3^2 \eta(w_1, w_5),$$

for all $\varphi := (\varphi_1, \varphi_2, \varphi_3, \varphi_4) \in \left[L^2(\Omega; H^1(Y))\right]^2 \times H_0^1(\Omega) \times L^2(\Omega; H^1(Y))$.

Lemma 2. *Let the assumptions (A1)–(A3) be satisfied. Then the weak solutions in the sense of Definition 1 are positive and bounded a.e. in Ω or, following the case, in $\Omega \times Y$.*

Proof. The conclusion of this result is obtained by choosing special test functions in Definition 1 in combination with a suitable application of Gronwall's lemma. □

Theorem 3 (Global existence and uniqueness)**.** *Let the assumptions (A1)–(A3) be satisfied and let $\tau > 0$ be arbitrarily chosen. Then problem (P) admits a unique positive and bounded (weak) solution such that*

$$w_3 \in w_3^D + L^2(0, \tau; H_0^1(\Omega)), \tag{9}$$

$$\partial_t w_3 \in L^2((0, \tau) \times \Omega), \tag{10}$$

$$(w_1, w_2, w_4) \in \left[L^2(0, \tau; L^2(\Omega, H^1(Y)))\right]^3, \tag{11}$$

$$(\partial_t w_1, \partial_t w_2, \partial_t w_4) \in \left[L^2((0, \tau) \times \Omega \times Y)\right]^3, \tag{12}$$

$$w_5 \in H^1(0, \tau; L^\infty(\Omega \times \{y = \ell\})). \tag{13}$$

Sketch of the proof. We obtain the existence of weak solutions to problem (P) relying on the two-scale Galerkin scheme developed in [20]. The idea is to exploit the special structure of the PDE system. In this way, the function spaces to be used for the (two-scale) Galerkin approximation of the solution can be chosen as tensor product of spaces on the macroscopic domain Ω and microstructure (local cell) Y. Sufficient uniform estimates for the finite dimensional approximations permit the convergence of the approximating sequence. Additionally, we can also prove the uniqueness of positive and bounded weak solutions to (P). □

Remark 4. It is worth noting that there are at least three other strategies than that sketched above, which are able to analyze this class of multiscale reaction-diffusion scenarios.

(i) The existence of weak solutions to (P) can also be obtained by means of a two-scale convergence approach done in combination with periodic homogenization procedure of the corresponding micro-sulfatation model that is behind (P); see [17] where a simplified scenario related to (P) has been treated via periodic homogenization. The reader is referred to [9] for a formal derivation of (P) (done for a locally-periodic choice of microstructures Y_x) and to [11] for basic results and nice worked-out examples of the application of rigorous periodic homogenization procedures to real-life situations.

(ii) Problem (P) can also dealt with in a more direct way, i.e. without a derivation via homogenization from a lower spatial scale. More precisely, it can be formulated as a Cauchy problem in a Hilbert space and resolved by holomorphic semigroups in the spirit of [24].

(iii) Trusting [15, 23], a suitable construction of a fixed-point operator can also provide the existence of weak solutions to (P).

2.4. Two-scale model with fast Henry-type transfer limit

We are interested in understanding the behavior of solutions to problem (P) as the mass-transfer Biot number Bi^M goes to infinity. In particular, we expect the solution $(w_1^\epsilon, w_2^\epsilon, w_3^\epsilon, w_4^\epsilon, w_5^\epsilon)$ of problem (P) to converge as

$$\epsilon := \frac{1}{Bi^M} \to 0 \tag{14}$$

to the solution $(u_1, u_2, u_3, u_4, u_5)$ of the following problem, say $(\tilde{P})$:

$$\beta_1 \partial_t u_1 - \beta_1 d_1 \Delta_y u_1 = -\Phi_1^2 k_1 u_1 + \Phi_2^2 k_2 u_2, \quad \text{in } \Omega \times Y \times S, \tag{15a}$$

$$\beta_2 \partial_t u_2 - \beta_2 d_2 \Delta_y u_2 = \Phi_1^2 k_1 u_1 - \Phi_2^2 k_2 u_2, \quad \text{in } \Omega \times Y \times S, \tag{15b}$$

$$\partial_t u_3 - d_3 \Delta u_3 = -d_2 \partial_y u_2|_{y=0}, \text{ in } \Omega \times S, \tag{15c}$$

$$\beta_4 \partial_t u_4 - \beta_4 d_4 \Delta_y u_4 = k_1 u_1, \text{ in } \Omega \times Y \times S, \tag{15d}$$

$$\beta_5 \partial_t u_5 = +\Phi_3^2 \eta(u_1, u_5), \quad \text{in } \Omega \times \{y = \ell\} \times S, \tag{15e}$$

with

$$
\begin{aligned}
&(16a) && -d_1\partial_y u_1 = 0, && \text{on } \Omega\times\{y=0\}\times S,\\
&(16b) && -d_1\partial_y u_1 = +\Phi_3^2\eta(u_1,u_5), && \text{on } \Omega\times\{y=\ell\}\times S,\\
&(16c) && u_2 = Hu_3, && \text{on } \Omega\times\{y=0\}\times S,\\
&(16d) && -d_2\partial_y u_2 = 0, && \text{on } \Omega\times\{y=\ell\}\times S,\\
&(16e) && u_3 = u_3^D, && \text{on } \Gamma^D\times S,\\
&(16f) && -d_3\partial_x u_3 = 0, && \text{on } \Omega\setminus\Gamma^D\times S,\\
&(16g) && -d_4\partial_y u_4 = 0, && \text{on } \Omega\times\{y=0\}\times S,\\
&(16h) && -d_4\partial_y u_4 = 0, && \text{on } \Omega\times\{y=\ell\}\times S,
\end{aligned}
$$

Note that (16c) is actually the well-known Henry's law. Following the terminology of Cook and Showalter [6], problem $(\tilde{P})$ is a *matched microstructure model*.

Remark 5. The analysis of problem $(\tilde{P})$ can be done in the same spirit as indicated in section 2.3.

3. Numerical scheme

In this section, we describe a semi-discrete numerical scheme for the problem (P) based on finite-difference discretization in space.

Let $h_x := L/N_x$ and $h_y := \ell/N_y$ be the spatial step sizes, where N_x and N_y are positive integers. Let $\Omega_h := \{x_i := ih_x \in \bar{\Omega} | i = 0,\dots,N_x\}$ and $Y_h := \{y_j := jh_y \in \bar{Y} | j = 0,\dots,N_y\}$ be uniform grids of nodes on Ω and Y, respectively. Also, let $\omega_h := \Omega_h \times Y_h$ and $\omega_h' := \Omega_h \times \{y_{N_y}\}$. We define sets of grid functions on Ω_h, ω_h and ω_h' as $\mathcal{G}_h^\Omega := \{u_h | u_h : \Omega_h \to \mathbb{R}\}$, $\mathcal{G}_h^\omega := \{v_h | v_h : \omega_h \to \mathbb{R}\}$ and $\mathcal{G}_h^{\omega'} := \{v_h | v_h : \omega_h' \to \mathbb{R}\}$, respectively, such that $u_i := u_h(x_i)$, $u_h \in \mathcal{G}_h^\Omega \cup \mathcal{G}_h^{\omega'}$ and $v_{ij} := v_h(x_i, y_j)$, $v_h \in \mathcal{G}_h^\omega$. Finally, we define the discrete Laplacian operators as $\Delta_h u_i := (u_{i-1} - 2u_i + u_{i+1})/h_x^2$, for $u_h \in \mathcal{G}_h^\Omega$, and as $\Delta_{Yh} v_{ij} := (v_{i,j-1} - 2v_{ij} + v_{i,j+1})/h_y^2$, for $v_h \in \mathcal{G}_h^\omega$.

A quintuple $\{w_h^k | k = 1,\dots,5\}$ with $w_h^k \in C^1([0,T],\mathcal{G}_h^\omega)$, $k \in \{1,2,4\}$, $w_h^3 \in C^1([0,T],\mathcal{G}_h^\Omega)$, $w_h^5 \in C^1([0,T],\mathcal{G}_h^{\omega'})$ is called a semi-discrete solution of the problem (P), if it satisfies the following system of ODEs

$$
\begin{aligned}
&(17a) && \beta_1\frac{\mathrm{d}w_{ij}^1}{\mathrm{d}t} = \beta_1 d_1\Delta_{Yh}w_{ij}^1 - \Phi_1^2 k_1 w_{ij}^1 + \Phi_2^2 k_2 w_{ij}^2,\\
& && \qquad i = 0,\dots,N_x,\ j = 0,\dots,N_y,\\
&(17b) && \beta_2\frac{\mathrm{d}w_{ij}^2}{\mathrm{d}t} = \beta_2 d_2\Delta_{Yh}w_{ij}^2 + \Phi_1^2 k_1 w_{ij}^1 - \Phi_2^2 k_2 w_{ij}^2,\\
& && \qquad i = 0,\dots,N_x,\ j = 0,\dots,N_y,\\
&(17c) && \frac{\mathrm{d}w_i^3}{\mathrm{d}t} = d_3\Delta_h w_i^3 - Bi^M\big(Hw_i^3 - w_{i,0}^2\big),\\
& && \qquad i = 1,\dots,N_x,\\
&(17d) && \beta_4\frac{\mathrm{d}w_{ij}^4}{\mathrm{d}t} = \beta_4 d_4\Delta_{Yh}w_{ij}^4 + k_1 w_{ij}^1,\\
& && \qquad i = 0,\dots,N_x,\ j = 0,\dots,N_y,\\
&(17e) && \beta_5\frac{\mathrm{d}w_i^5}{\mathrm{d}t} = \Phi_3^2\eta\big(w_{i,N_y}^1, w_i^5\big),\ i = 0,\dots,N_x,
\end{aligned}
$$

for $t > 0$, together with the initial conditions

$$
(17f) \qquad w_h^k(0) = \mathcal{P}_h^k w_{k0},\ k = 1,\dots,5,
$$

where $\mathcal{P}_h^k$ denotes projection operators that project continous functions w_{k0} on the corresponding grids.

Values of grid functions on nodes outside the grids, that arise in (17), are eliminated using centered difference approximations of the boundary conditions (5). Thus, for these values and for the Dirichlet boundary condition we obtain the following relations

$$
\begin{aligned}
&(18a) && w_{i,-1}^1 = w_{i,1}^1, && i = 0,\dots,N_x,\\
&(18b) && w_{i,N_y+1}^1 = w_{i,N_y-1}^1 - \frac{2h_y\Phi_3^2}{d_1}\eta\big(w_{i,N_y}^1, w_i^5\big), && \\
& && \qquad i = 0,\dots,N_x,\\
&(18c) && w_{i,-1}^2 = w_{i,1}^2 + \frac{2h_y Bi^M}{d_2}\big(Hw_i^3 - w_{i,0}^2\big), && \\
& && \qquad i = 0,\dots,N_x,\\
&(18d) && w_{i,N_y+1}^2 = w_{i,N_y-1}^2, && i = 0,\dots,N_x,\\
&(18e) && w_0^3 = w_3^D, && \\
&(18f) && w_{N_x+1}^3 = w_{N_x-1}^3, && \\
&(18g) && w_{i,-1}^4 = w_{i,1}^4, && i = 0,\dots,N_x,\\
&(18h) && w_{i,N_y+1}^4 = w_{i,N_y-1}^4, && i = 0,\dots,N_x,
\end{aligned}
$$

for $t > 0$.

4. Numerical results

In this section we present numerical results illustrating the behavior of solutions to the problem (P).The numerical results for the problem (P) were obtained by integrating the initial value problem (17), (18) in time by means of the toolbox CVODE [5].

We perform the numerical experiments on $\Omega = (0,10)$ and $Y = (0,1)$. The computational grid is chosen so that $N_x = N_y = 128$, unless stated otherwise. The relative and absolute tolerance for the CVODE solver is set to the value of 10^{-9}. We assume zero constant initial conditions for $w_h^k(0)$, $k = 2,4,5$ (i.e., there is no initial concentration of H_2S, moisture and gypsum, respectively), while we assume $w_h^1(0) = 0.01$ (i.e., low initial concentration of H_2SO_4). The value of the initial concentration $w_h^3(0)$ is chosen to be compatible with the Dirichlet boundary condition $w_3^D = 0.011$. The values of the remaining parameters which are common to all presented numerical experiments are summarized in Table 1.

4.1. Rate of convergence of the scheme (17) for $h \to 0$

In this paragraph we present results of measuring the experimental order of convergence of the scheme (17) as the spatial size of the computational mesh decreases to zero. As there is no analytical solution available with which we

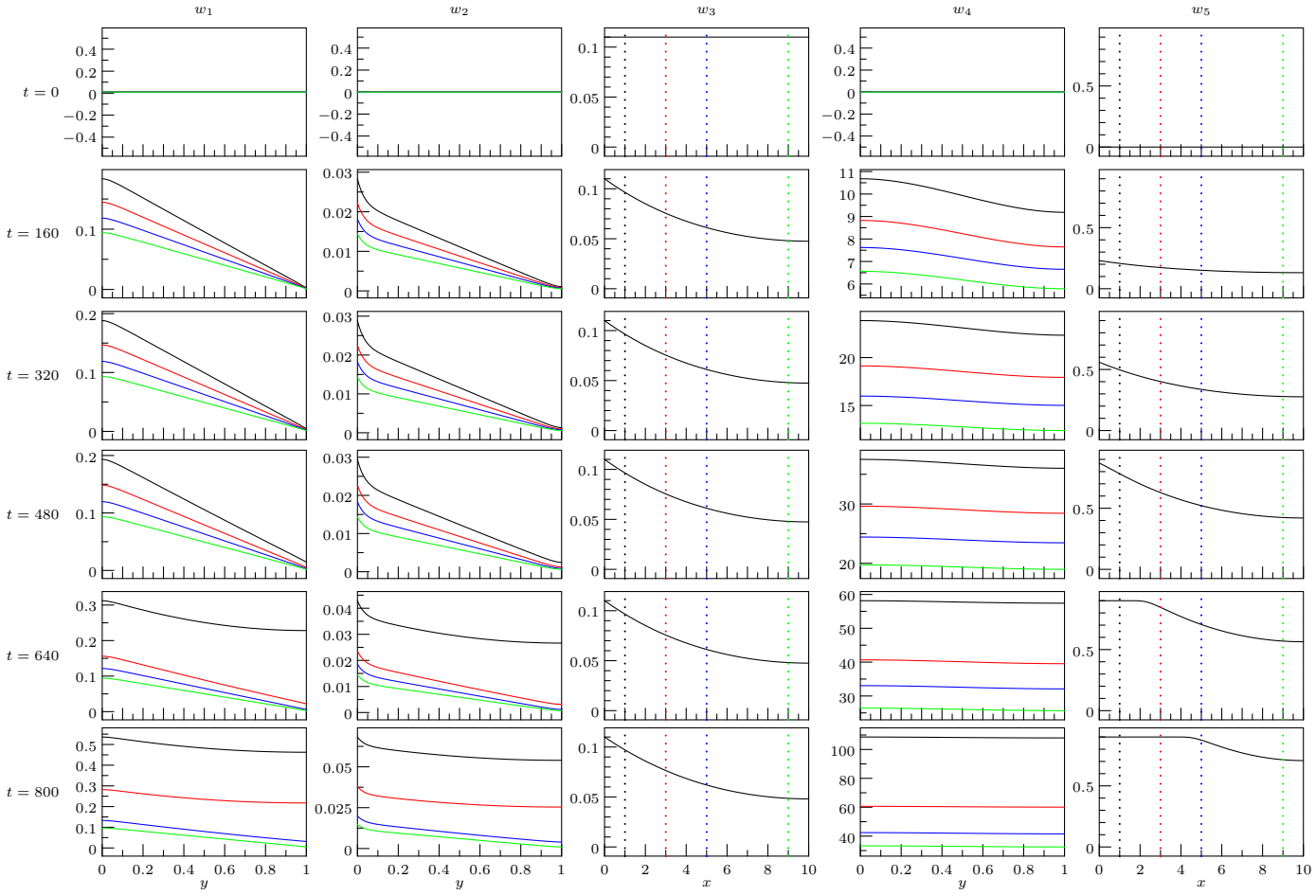

Figure 1: Plots of the time evolution of the semi-discrete solution to problem (P) computed with the scheme (17) for $Bi^M = 0.00864$.

β_i	k_1	k_2	k_3	$d_{1,2,4}$	d_3	$\bar{c}$	H	p	q	Φ_2^i
1	0.84	7.2	1.0	0.00864	0.864	0.9	2.5	1	1	1

Table 1: Reference set of parameter values. They are used in all presented numerical experiments.

can compare the approximate solution, we use a so-called double-mesh principle: we consider a set of gradually refined meshes whose number of mesh nodes N_x, N_y is chosen so that $N_x = N_y = 2^N$, where $N = 5, \ldots, 9$. Then we measure the convergence by comparing the error of approximate solutions obtained on two successive meshes, i.e., meshes with the spatial step sizes $h := (h_x, h_y)$ and $h/2 := (h_x/2, h_y/2)$.

We define the discrete error at time T as a grid function e_h^k in the following way:

$$(e_h^k)_i := (w_h^k)_i(T) - (w_{h/2}^k)_{2i}(T), \tag{19}$$

for $k \in \{3, 5\}$ and

$$(e_h^k)_{ij} := (w_h^k)_{ij}(T) - (w_{h/2}^k)_{2i,2j}(T), \tag{20}$$

for $k \in \{1, 2, 4\}$.

To quantify the error, we define the following discrete L^2-norms and maximum norms so that

$$\|e_h^k\|_2^2 := \frac{h_x}{2} \sum_{i=0}^{N_x-1} \left((e_i^k)^2 + (e_{i+1}^k)^2\right), \tag{21}$$

$$\|e_h^k\|_\infty := \max_{x_i \in \Omega_h} |e_i^k|, \tag{22}$$

for $k \in \{3, 5\}$ and

$$\|e_h^k\|_2^2 := \frac{h_x h_y}{4} \sum_{i=0}^{N_x-1} \sum_{i=0}^{N_y-1} \left((e_{ij}^k)^2 + (e_{i+1,j}^k)^2 + (e_{i,j+1}^k)^2 + (e_{i+1,j+1}^k)^2\right), \tag{23}$$

$$\|e_h^k\|_\infty := \max_{x_{ij} \in \mathcal{G}_h^{\omega'}} |e_{ij}^k|, \tag{24}$$

for $k \in \{1, 2, 4\}$.

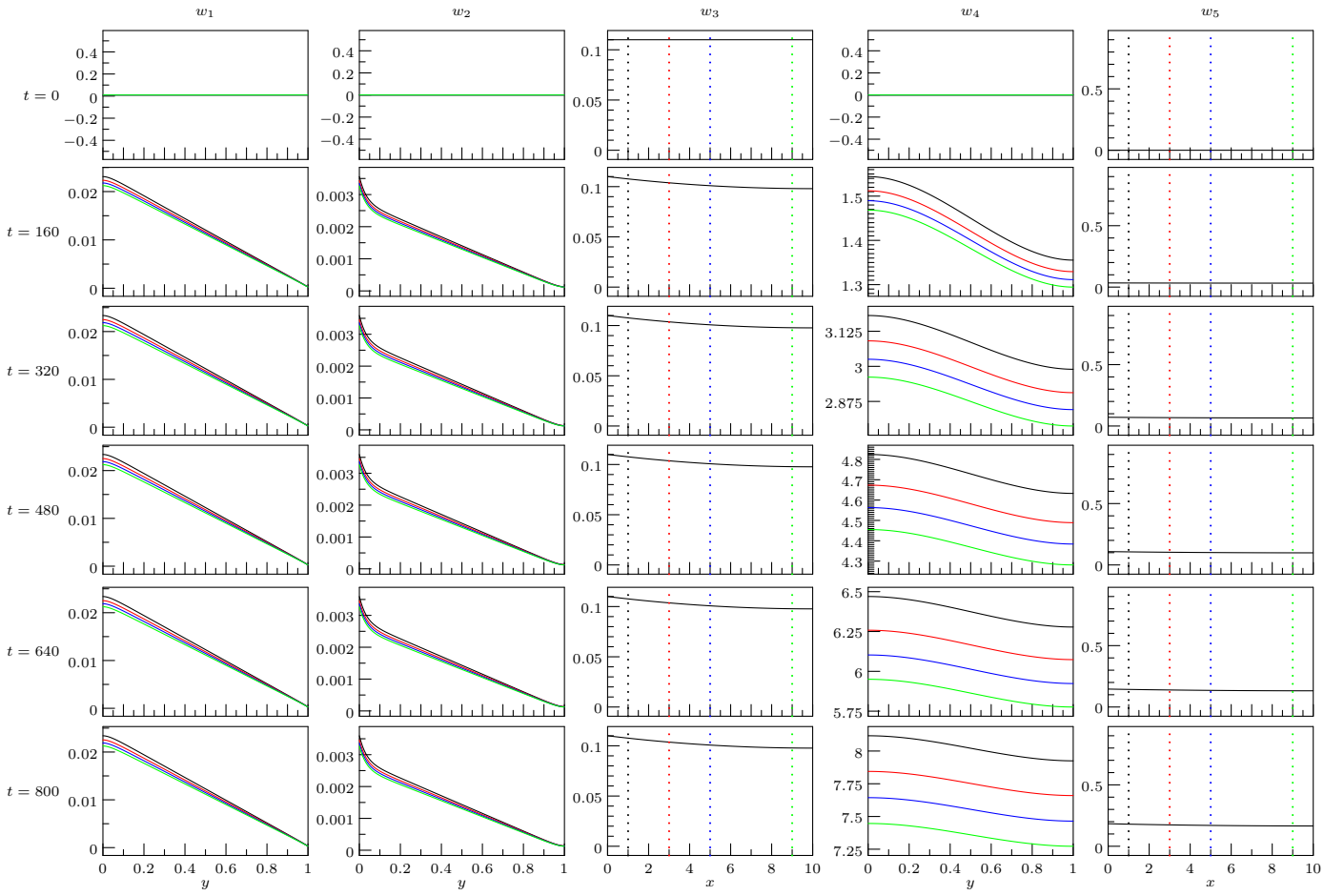

Figure 2: Plots of the time evolution of the semi-discrete solution to problem (P) computed with the scheme (17) for $Bi^M = 0.000864$.

Finally, we define the experimental order of convergence EOC_p^k of w_h^k as

$$EOC_p^k := \log_2 \left(\frac{\|e_h^k\|_p}{\|e_{h/2}^k\|_p} \right). \tag{25}$$

Using these definitions we performed the analysis of the rate of convergence for w_h^k, $k = 1, \ldots, 5$. We set $L_x = L_y = 1$ to obtain equal spatial step sizes in both directions and we evolved the solution until $T = 80$. Also, to minimize the influence of the truncation error from the time integration, we set the relative and absolute tolerance to a stringent value of 10^{-13}. The Biot number Bi^M was set equal to 86.4 and the values of the remaining parameters are given in Table 1. The results of the EOC computations are given in Table 2 where the error is measured in L^2-norms (21), (23) and in Table 3 where the error is measured in maximum norms (22), (24). In the first column the number of mesh nodes N in one direction is shown (the corresponding spatial step size is thus $h_x = h_y = 1/2^N$). In the following columns we show the norm of the error function for each w_h^k, $k \in \{1, \ldots, 5\}$ together with the EOC.

From the obtained results we can conclude that, with very high probability, the scheme converges with second-order accuracy.

4.2. Illustration of concentration profiles for $\epsilon > 0$

We next present several computations in order to demonstrate the behavior of the system (P) for various values of the parameter ϵ defined by (14), that is, for various values of Bi^M. We used parameter values as described at the beginning of this Section and in Table 1. We evolved the solution until $T = 800$.

The numerical solutions are presented in the figures in the following way. In the columns, the time evolution of each of the functions w_k is shown and each row corresponds to one time moment (displayed at left) with the top row showing the initial conditions. We plot functions w_k, $k \in \{1, 2, 4\}$, defined on $\Omega \times Y$ as functions of y for four fixed values of $x \in X := \{1, 3, 5, 9\}$ (i.e., we plot the profiles of these functions at pores located at the specified x positions). The position of these values of x is shown in the third and fifth column as colored vertical dotted lines and the color of each dotted line matches the color of the

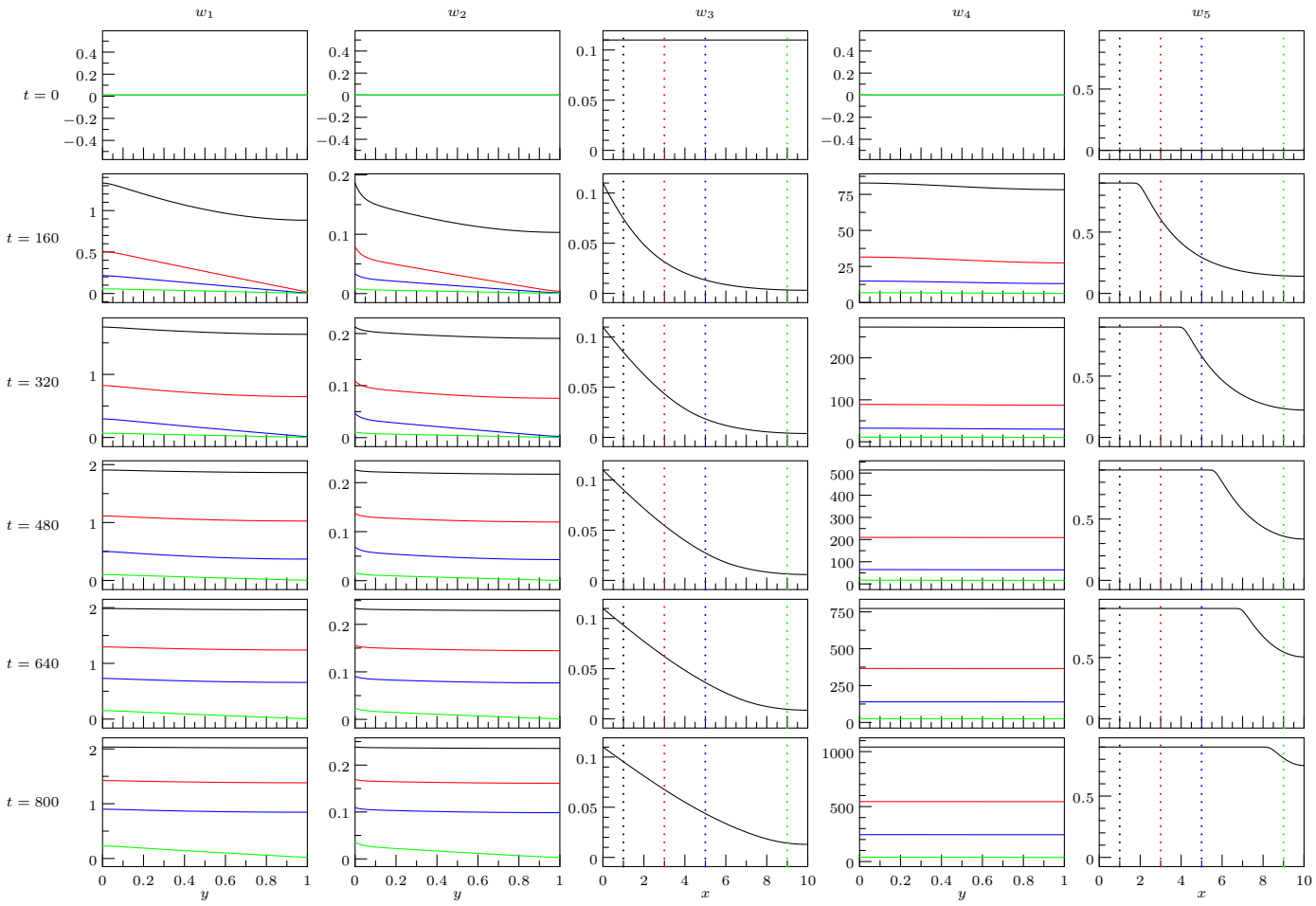

Figure 3: Plots of the time evolution of the semi-discrete solution to problem (P) computed with the scheme (17) for $Bi^M = 864$.

graph of the functions $w_k(x,\cdot)$, $k \in \{1,2,4\}$, $x \in X$, in the first, second and fourth column.

The result of the first computation is shown in Fig. 1 where $Bi^M = 0.00864$ ($\epsilon \approx 115.741$). We also use this example to describe a typical behavior of the solution of the system (2). Starting with the middle column displaying the evolution of w_3 we see that at the onset of the simulation, the initially constant concentration of H_2S in the air phase decreases rapidly as it enters through the water-air interface into the water phase at each pore unsaturated by H_2S. The concentration of H_2S in the sewer atmosphere is assumed constant and is modelled by the Dirichlet boundary condition at $x = 0$. After entering into the water phase, H_2S diffuses and undergoes a reaction that converts it into H_2SO_4. This evolution is depicted in the second column. The w_2 attains higher values at lower x position (closer to the inner surface of the pipe) copying at $y = 0$ the profile of w_3.

The concentration of H_2SO_4 (i.e., w_1) is plotted in the first column. At first w_1 has a nearly linear profile for each fixed x decreasing to almost zero at the water-concrete interface ($y = \ell$) where it is consumed by the chemical reaction (1d) that converts concrete into gypsum. This conversion can be seen in the fifth column which shows the evolution of the gypsum concentration w_5. At the beginning, the concrete is not damaged and $w_5 = 0$. Increased concentration of w_1 at $y = \ell$ results in growing concentration of w_5, this process being at first more noticeable closer to the surface of the pipe. The w_5 continues to grow until it reaches a critical value $\bar{c} = 0.9$ which can be interpreted as an indication of complete conversion of concrete into gypsum.

Once w_5 reaches $\bar{c}$, w_1 is not consumed anymore in the concrete corrosion and the boundary condition at $y = \ell$ changes into no-flux condition. At $t = 640$ this change has taken place at $x = 1$ and is about to take place at $x = 3$. As can be seen in the first column, as a consequence of this change, w_1 starts to grow at $x = 1$ gradually approaching a constant value over all Y. At $t = 800$ the corrosion front has nearly arrived at $x = 5$: the profiles of w_1 corresponding to $x = 1$ and $x = 3$ have already grown and the one corresponding to $x = 5$ is now starting to grow. The growth of w_1 results in the growth of w_2 which in turn results in a slow growth of w_3. Finally, the fourth column shows the

N	$\|e_h^1\|_2$	EOC_2^1	$\|e_h^2\|_2$	EOC_2^2	$\|e_h^3\|_2$	EOC_2^3	$\|e_h^4\|_2$	EOC_2^4	$\|e_h^5\|_2$	EOC_2^5
32	0.01929	1.85569	0.00216	1.85466	0.00009	1.80801	0.98538	1.83429	0.01368	1.77918
64	0.00533	1.96049	0.00060	1.96036	0.00003	1.94844	0.27633	1.95547	0.00399	1.94165
128	0.00137	1.98988	0.00015	1.98986	0.00001	1.98686	0.07125	1.98865	0.00104	1.98519
256	0.00034		0.00004		0.00000		0.01795		0.00026	

Table 2: Results of our convergence rate study (measured in the discrete L^2-norm).

N	$\|e_h^1\|_\infty$	EOC_∞^1	$\|e_h^2\|_\infty$	EOC_∞^2	$\|e_h^3\|_\infty$	EOC_∞^3	$\|e_h^4\|_\infty$	EOC_∞^4	$\|e_h^5\|_\infty$	EOC_∞^5
32	0.04280	1.98990	0.00417	1.99067	0.00012	1.80827	1.27092	1.83487	0.01411	1.79127
64	0.01078	2.00096	0.00105	2.00400	0.00003	1.94850	0.35626	1.95564	0.00408	1.94369
128	0.00269	2.00047	0.00026	2.00091	0.00001	1.98687	0.09185	1.98869	0.00106	1.98563
256	0.00067		0.00007		0.00000		0.02314		0.00027	

Table 3: Results of our convergence rate study (measured in the discrete maximum norm).

evolution of w_4 – moisture as a product of reaction decomposing H_2SO_4. As the time increases, the corrosion tends to be complete and apparently the system wants to reach a constant steady state.

In Fig. 2, we show a computation with a Biot number much lower than in the previous numerical experiment– here $Bi^M = 0.000864$ ($\epsilon \approx 1157.407$). Consequently, the coupling between the equations for w_3 and w_2 becomes looser. As a result, w_3 does not decrease as much as in the previous experiment due to a *barrier* for H_2S in the air hindering its entrance into the water phase. Hence w_2 and w_1 attain lower values and their profiles tend to be uniform along the x-axis. Eventually, this leads to a slow, gradual corrosion of the pipe wall simultaneously along the whole domain and we do not observe the same progress of the corroding front as in the previous case (there is nearly no motion of the corrosion front).

Fig. 3 shows a computation with a much larger Biot number compared to the both previous experiments. Here we used $Bi^M = 864$ ($\epsilon \approx 0.00116$), which means that the boundary condition for w_2 at $y = 0$ is essentially a Dirichlet one. We can observe that in this case the concentrations of w_2 and w_3 are higher than in the previous numerical experiments. Additionally, the corrosion process seems to be much faster exhibiting a prominent corroding front (observable in the fifth column) advancing into the concrete.

4.3. Illustration of the convergence scenario: $\epsilon \to 0$

In this paragraph we are concerned with the behavior of solutions to (P) as $\epsilon \to 0$. The main result here is that we show numerically that

$$\|Hw_3 - w_2|_{y=0}\|_{L^2(\Omega)} \to 0 \text{ as } \epsilon \to 0,$$

i.e., as $Bi^M \to \infty$. We show this by simply measuring the experimental order of convergence. We plan to prove rigorously this behavior elsewhere. We proceed as follows: We compute solutions of (17) at $T = 800$ for gradually increasing values of $Bi^M = 4^i$, $i \in \{1, \dots, 6\}$. For each choice of ϵ, we measure the quantity $E_\epsilon := \|Hw_h^3(T) - w_h^2(T)|_{\Omega_h}\|_2$ in terms of the discrete L^2-norm; see (21). Finally, we define the experimental order of convergence of E_ϵ as

$$EOC_{E_\epsilon} := \frac{\log(E_{\epsilon_1}) - \log(E_{\epsilon_2})}{\log(\epsilon_1) - \log(\epsilon_2)}. \tag{26}$$

The results shown in Table 4 indicate that E_ϵ behaves as $O(\epsilon)$.

$\log_4 Bi^M$	$\left\|Hw_h^3 - w_h^2\|_{\Omega_h}\right\|_2$	EOC_{E_ϵ}
-2	$6.95208 \cdot 10^{-2}$	0.98907
-1	$1.76455 \cdot 10^{-2}$	0.98806
0	$4.48495 \cdot 10^{-3}$	0.99612
1	$1.12728 \cdot 10^{-3}$	0.99896
2	$2.82225 \cdot 10^{-4}$	0.99973
3	$7.05819 \cdot 10^{-5}$	0.99993
4	$1.76471 \cdot 10^{-5}$	0.99998
5	$4.41187 \cdot 10^{-6}$	0.99999
6	$1.10297 \cdot 10^{-6}$	

Table 4: Experimental order of convergence of E_ϵ as $\epsilon \to 0$.

5. Discussion

The results of section 4.3 encourage us to ask the questions:

(Q1) Do the concentration profiles corresponding to (P) approach those corresponding to $(\tilde{P})$ as ϵ goes to zero? If yes, then in which sense?

(Q2) For suitable parameter regimes, have the solutions to problems (P) and $(\tilde{P})$ the *same* large-time behavior?

Trusting the analysis by Cook and Showalter reported in [6], we expect a positive answer to the question (Q1). However, we need to take into account the specifics of (P) and

check which regularity of data and parameters is required for the limit $Bi^M \to \infty$ to make sense.

To answer (Q2), we would need to do more numerical experiments. From the analysis point of view, we expect the existence of constant steady states. Again, it remains to investigate what are the necessary and sufficient conditions that both problems have the same constants as the steady states.

Following the line opened by [19, 20], we are very much interested in analyzing from a rigorous perspective the effect of the choice of micro-macro transmission conditions on the quality of the multiscale FD scheme described in section 3. More precisely, we will address elsewhere questions related to finding *a priori* and *a posteriori* error estimates for such class of two-scale reaction-diffusion systems.

Acknowledgments

We acknowledge fruitful discussions with Maria Neuss-Radu (Heidelberg), Toyohiko Aiki (Gifu), Omar Lakkis (Sussex), Jens Kruschwitz (Bochum), and Robin Beddoe (München). A. M. thanks Michael Böhm (Bremen) and the researchers team involved in the DFG priority program SPP 1122 for introducing him to the modeling of concrete-based materials. V. Ch. was supported by Global COE Program "Education and Research Hub for Mathematics-for-Industry" from the Ministry of Education, Culture, Sports, Science and Technology, Japan.

References

[1] Aregba-Driolett, D., Diele, F., and Natalini, R.: A mathematical model for the SO_2 aggression to calcium carbonate stones: Numerical approximation and asymptotic analysis, *SIAM J. Appl. Math.* **64**(5) (2004), 1636–1667.

[2] Balls, P. W., and Liss, P. S.: Exchange of H_2S between water and air, *Atmosphere Environment* **17** (1983), 737–742.

[3] Beddoe, R. E., and Dorner, H. W.: Modelling acid attack on concrete: Part 1. The essential mechanisms, *Cement and Concrete Research* **35** (2005), 2333–2339.

[4] Böhm, M., Jahani, F., Devinny, J., and Rosen, G.: A moving-boundary system modeling corrosion of sewer pipes, *Appl. Math. Comput.* **92** (1998), 247–269.

[5] Cohen, S. D., and Hindmarsh, A. C.: CVODE, a stiff/nonstiff ODE solver in C, *Computers in Physics* **10** (1996), 138–143.

[6] Cook, J. D., and Showalter, R. E.: Microstructure diffusion models with secondary flux, *J. Math. Anal. Appl.* **189** (1995), 731–756.

[7] Danckwerts, P. V.: *Gas-Liquid Reactions*, McGraw-Hill, New York, 1970.

[8] Eck, Ch.: Homogenization of a phase field model for binary mixtures, *Multiscale Modeling and Simulation* **3**(1) (2004), 1–27.

[9] Fatima, T., Arab, N., Zemskov, E. P., and Muntean, A.: Homogenization of a reaction-diffusion system modeling sulfate corrosion in locally-periodic perforated domains, *J. Engng. Math.* (2010) (to appear).

[10] Hewlett, P. C.: *Lea's Chemistry of Cement and Concrete (Fourth Edition)*, Butterworth-Heinemann, Oxford, 2003.

[11] Hornung, U. (Ed.): *Homogenization and Porous Media*, Interdisciplinary Applied Mathematics, Vol. 6, Springer-Verlag, New York, 1997.

[12] Jahani, F., Devinny, J., Mansfeld, F., Rosen, I. G., Sun, Z., and Wang, C.: Investigations of sulfuric acid corrosion of the concrete, I: Modeling and chemical observations, *J. Environ. Eng.* **127**(7) (2001), 572–579.

[13] Jahani, F., Devinny, J., Mansfeld, F., Rosen, I. G., Sun, Z., and Wang, C.: Investigations of sulfuric acid corrosion of the concrete, II: Electrochemical and visual observations, *J. Environ. Eng.* **127**(7) (2001), 580–584.

[14] Marchand, J., Samson, E., Maltais, Y., Lee, R. J., and Sahu, S.: Predicting the performance of concrete structures exposed to chemically aggressive environment-field validation, *Materials and Structures* **35** (2002), 623–631.

[15] Meier, S. A.: Two-scale models for reactive transport and evolving microstructure, Ph.D. thesis, University of Bremen, Germany, 2008.

[16] Meier, S. A., and Muntean, A.: A two-scale reaction-diffusion system with micro-cell reaction concentrated on a free boundary, *Comptes Rendus Mécanique* **336**(6) (2009), 481–486.

[17] Meier, S. A., and Muntean, A.: A two-scale reaction-diffusion system: Homogenization and fast-reaction limits, *Gakuto Int. Ser. Math. Sci. Appl.* **32**(2010), Current Advances in Nonlinear Analysis and Related Topics, 443–461.

[18] Meier, S. A., Peter, M. A., Muntean, A., Böhm, M., and Kropp, J.: A two-scale approach to concrete carbonation, in: *Proc. International RILEM Workshop on Integral Service Life Modelling of Concrete Structures*, RILEM Publications, 2007, pp. 3–10.

[19] Muntean, A., and Lakkis, O.: Rate of convergence for a Galerkin scheme approximating a two-scale reaction-diffusion system with nonlinear transmission condition, *CASA Report* No. 10-08, Eindhoven: Technische Universiteit Eindhoven, 2010.

[20] Muntean, A., and Neuss-Radu, M.: A multiscale Galerkin approach for a class of nonlinear coupled reaction-diffusion systems in complex media, *J. Math. Anal. Appl.* (2010) doi:10.1016/j.jmaa.2010.05.056.

[21] Müllauer, W., Beddoe, R. E., and Heinz, D.: Sulfate attack on concrete – Solution concentration and phase stability, in: *Concrete in Aggressive Aqueous Environments, Performance, Testing and Modeling*, RILEM Publications, 2009, pp. 18–27.

[22] Neville, A.: The confused world of sulfate attack on concrete, *Cement and Concrete Research* **34** (2004), 1275–1296.

[23] Noorden, T. L. van, and Muntean, A.: Homogenization of a locally-periodic medium with areas of low and high diffusivity, *CASA Report* No. 10-19, Eindhoven: Technische Universiteit Eindhoven, 2010.

[24] Showalter, R. E., and Walkington, N. J.: Microstructure models of diffusion in fissured media, *J. Math. Anal. Appl.* **155** (1991), 1–20.

[25] Song, H. W., Lim, H. J., Saraswathy, V., and Kim, T. H.: A micro-mechanics based corrosion model for predicting the service life of reinforced concrete structures, *Int. J. Elect. Sci.* **2** (2007), 341–354.

[26] Taylor, H. F. W.: *Cement Chemistry*, Academic Press, London, 1990.

[27] Tixier, R., Mobasher, B., and Asce, M.: Modeling of damage in cement-based materials subjected to external sulfate attack. I: Formulation, *J. Mat. Civil Engng.* **15** (2003), 305–313.

[28] Weber, W. A., and DiGiano, F. A.: *Process Dynamics in Environmental Systems*, Wiley, New York, 1996.

Vladimír Chalupecký
Faculty of Mathematics, Kyushu University, Fukuoka, Japan
E-mail: chalupecky@math.kyushu-u.ac.jp

Tasnim Fatima
CASA – Centre for Analysis, Scientific computing and Applications, Department of Mathematics and Computer Science, Technical University Eindhoven, Netherlands
E-mail: t.fatima@tue.nl

Adrian Muntean
CASA – Centre for Analysis, Scientific computing and Applications, Institute for Complex Molecular Systems (ICMS), Department of Mathematics and Computer Science, Technical University Eindhoven, Netherlands
E-mail: a.muntean@tue.nl